Reduced surface effects in weakly interacting ZrO_2 coated $MnFe_2O_4$ nanoparticles

F. Zeb[a], M. Ishaque[a], K. Nadeem[a*], M. Kamran[a], H. Krenn[b], D. V. Szabo[c, d], U. Brossmann[e], I. Letofsky-Papst[f]

[a] *Nanoscience and Technology Laboratory, International Islamic University, Islamabad 44000, Pakistan*

[b] *Institute of Physics, Karl-Franzens University, Universitätsplatz 5, A-8010 Graz, Austria*

[c] *Institute for Applied Materials, Karlsruhe Institute of Technology (KIT), D-76344 Eggenstein-Leopoldshafen, Germany*

[d] *Karlsruhe Nano Micro Facility (KNMF), Karlsruhe Institute of Technology (KIT), D-76344 Eggenstein-Leopoldshafen, Germany*

[e] *Institute of Materials Physics, University of Technology Graz, A-8010 Graz, Austria*

[f] *Institute for Electron Microscopy, University of Technology Graz, Steyrergasse 17, A-8010 Graz, Austria*

[*] *Corresponding author's e-mail: kashif.nadeem@iiu.edu.pk (K. Nadeem)*

Phone # 0092-51-9019714

Abstract

Surface effects in zirconium dioxide (ZrO_2) coated manganese ferrite ($MnFe_2O_4$) nanoparticles have been studied by using dc and ac magnetization. The average crystallite size of $MnFe_2O_4$ and ZrO_2 phase was about 9 and 4 nm, respectively as determined by Debye-Scherrer´s formula. TEM images revealed that the nanoparticles are spherical in shape with less agglomeration. Selected area electron diffraction analysis shows two different crystalline species such as nanoparticle's core $MnFe_2O_4$ and coating ZrO_2, which was in agreement with the XRD analysis. Effective anisotropy constant (K_{eff} = 3 x 10^{04} erg/cm^3) as deduced from simulated ZFC/FC curves is close to bulk value (K_{bulk} = 2.5 x 10^{04} erg/cm^3) which is due to weak contribution of surface anisotropy. Saturation magnetization showed an increasing trend at low temperatures (more

pronounced below 50 K) which is again due to reduced surface spins disorder. Temperature dependent coercivity revealed a sharp increase at 5K, which is due to the surface spins freezing. The Arrhenius law fit to frequency shift of T_B in ac susceptibility revealed weak interparticle interactions. The nanoparticles showed slow spin relaxation in ZFC protocol which signify the presence of disorder in our nanoparticles, however the value of shape parameter β lies outside the spin-glass regime. In summary, non-magnetic ZrO_2 coating on these fine $MnFe_2O_4$ nanoparticles reduces their surface energy, magnetic interparticle interactions and surface effects, which are not sufficient to establish a spin-glass behaviour.

Key Words: Manganese ferrite; Spin glass; Coating; Zirconia

1. Introduction

Among the ferrimagnetic spinel ferrites, manganese ferrite ($MnFe_2O_4$) is one of the soft ferrite with promising applications due to their large resistivity, permeability, high saturation magnetization, small coercivity and moderate magnetocrystalline anisotropy. Soft ferrites are best candidates for applications such as microwave devices, transformer cores, ferro-fluids and telecommunication [1-4]. According to the cationic distribution, manganese ferrite ($MnFe_2O_4$) has partially inverse spinel structure [5, 6]. At nanoscale, $MnFe_2O_4$ shows reduced magnetization as compared to bulk due to reduced bonds and frustration of the exchange coupling between ferrimagnetically coupled spins near the surface of the individual nanoparticle. This surface disorder sometimes becomes strong enough to produce surface spin-glass behavior in ferrite nanoparticles [7, 8].

In addition to surface spin-glass, magnetic nanoparticles also exhibit superparamagnetism which is usually manifested by the existence of blocking temperature. Thermal energy and magneto-crystalline anisotropy energy are the competing mechanism for superparamagnetism. This phenomenon is usually observed in small-sized nanoparticles, where thermal energy exceeds the

magneto-crystalline energy barrier that flips the spins more frequently. In nanoparticles, blocking and spin-glass transition temperatures are usually overlapped [9], which makes them difficult to distinguishable. However by using indirect experimental evidences, now it is well established to distinguish between superparamagnetism and spin-glass behavior in magnetic nanoparticles [10]. Ferrite magnetic nanoparticles also contribute random interparticle dipolar interactions which can also lead to spin-glass behavior known as super spin-glass. Kodama *et al.* [11] proposed a surface spin-glass freezing model which are based on surface disorder arises due to the existence of broken bonds and as a result it reduced the saturation magnetization (M_S) of the nanoparticles. Lartigue *et al.* [12] reported the existence of super-spin glass behavior in Fe_3O_4 nanoparticles, but an enhancement of M_S is observed, which arises from both inter-particle dipolar and exchange coupling. Gao *et al*. [13] synthesized $MnFe_2O_4$ nanoparticles by the thermal decomposition method and reported surface spin-glass like state. Ghosh *et al.* [14] studied the PVA capped Fe_3O_4 nanoparticles and reported spin glass type transition at 125 K.

It is desirable to reduce the interparticle interactions to study the surface effects in ferrite nanoparticles. Suitable non-magnetic surface coating can be useful in reducing the interparticle interactions and agglomeration. Non-magnetic surface coating can also reduce the surface energy of the ferrite nanoparticles and surface disorder can be minimised. Aslibeiki *et al.* [15] synthesized $MnFe_2O_4$ nanoparticles by using different contents of tri-ethylene glycol and found that polymer coating can enhance the M_S value by reducing the surface spins disorder and lower the blocking temperature with remarkable shift. Rashid *et al.* [16] reported that the ZrO_2 coated $MgFe_2O_4$ nanoparticles are useful for hyperthermia applications. Girija *et al.* [17] reported that ZrO_2 coating prevents the aggregation among Fe nanoparticles. However, some non-magnetic coating can enhance the surface effects as reported by Larumbe *et al.* [18] in SiO_2 coated $NiFe_2O_4$ nanoparticles.

In this work, we have preferred non-magnetic ZrO_2 as a coating material to reduce the agglomeration, interparticle interactions and surface disorder. ZrO_2 is one of the material that exhibits remarkable properties such as high melting point, low thermal conductivity at room temperature, excellent chemical and corrosion resistance, high refractive index, large band gap, high dielectric constant, and bio-compatibility. Its stability at room temperature makes it stable against agglomeration and surface disorder. It can also restrict the growth of nanoparticles as observed by Xu *et al.* [19] in ZrO_2 coated FePt nanoparticles.

2. Experimental

$MnFe_2O_4$ nanoparticles coated with ZrO_2 and protected by poly methyl methacrylate (PMMA) were prepared by microwave plasma synthesis [20, 21]. Fig. 1 shows the schematic diagram for the preparation of these nanoparticles by using microwave plasma synthesis method. For synthesis of ZrO_2 coated nanoparticles, a 2.45 GHz microwave equipment with commercial components as microwave generator, magnetron, isolator, directional coupler and tri-stub-tuner (Muegge, Reichelsheim, Germany), and specially designed cavities, using the rotating TE_{11}-mode in consecutive arrangement were used. The diameter of the used quartz glass reaction tube was 28 mm. The length of the plasma zone was 12 cm, which approximately corresponds to one wavelength λ of the 2.45 GHz microwaves.

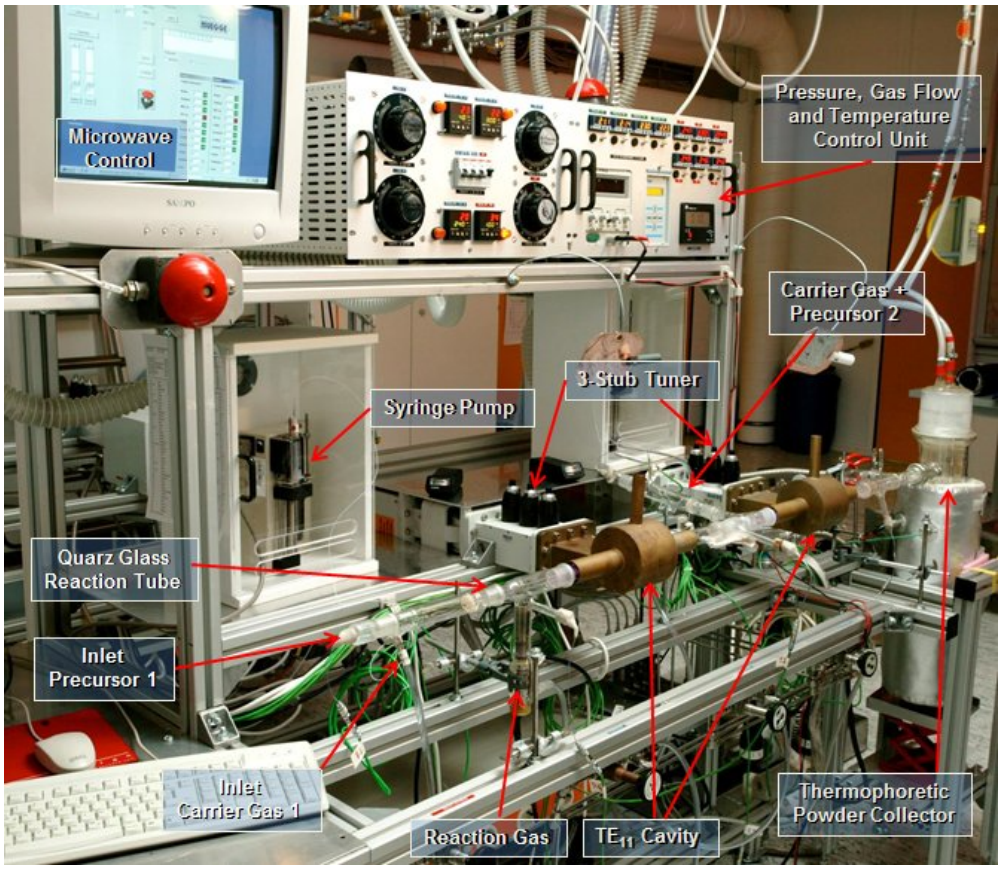

Fig. 1: Experimental setup for the synthesis of ZrO_2 coated $MnFe_2O_4$ nanoparticles.

1 g of solid $Mn_2(CO)_{10}$ and 2.1g of liquid $Fe(CO)_5$ were mixed, yielding 2 ml of liquid precursor, fed with a rate of 20 ml/h using a syringe pump, evaporated at 160 °C and transported with 0.2 lpm Ar carrier gas into the reaction system just before the plasma zone, where formation of the core nanoparticles occurs. In parallel, for the ZrO_2 coating 1.6 g of $ZrCl_4$ was used as the precursor, and evaporated at 280°C outside the reaction zone. The preheated precursor gas was transported with 0.2 lpm Ar-carrier gas into the plasma zone for the formation of ZrO_2 coating. Plasma and reaction gas is a mixture of Ar /20% O_2 with a 7.5 lpm gas flow rate. The pressure in the system was set to 2 mbar by using two vacuum pumps. The microwave power was set to 2000 W, corresponding to reaction temperature around 350°C. Electric charging of the particles induced by the plasma in combination with short residence time of only a few milliseconds and the low reaction temperatures prevent the

formation of hard agglomerates during synthesis. The nanoparticles were collected via thermophoresis on a cold finger. This powder was subsequently scraped off with a razor blade. The structural characterization of powder samples recorded with radiation Cu-Kα (λ = 0.154 nm) (Bruker D8 Advance instrument) at room temperature. Transmission electron microscopy (TEM) was used for nanoparticle's imaging. The magnetic properties were done by using a superconducting quantum interference device (SQUID)-magnetometer (Quantum Design, MPMS-XL-7).

3. Results and Discussion

Fig. 2 (a) shows the X-ray diffraction (XRD) scan of ZrO_2 coated $MnFe_2O_4$ nanoparticles placed on aluminum substrate. In this pattern, aluminum substrate was used to support the sample for measurement whose peaks are represented by Miller indices (111), (200), (220) and (311) at scattering angles of 38.5°, 45°, 65° and 77°, respectively. The XRD peaks at ($\bar{1}$11), (211) and (302) correspond to monoclinic phase of ZrO_2 (m-ZrO_2). Peaks at (111) and (220) correspond to main cubic phase of ZrO_2 (c-ZrO_2). The diffraction peaks of $MnFe_2O_4$ fit perfectly with the standard data of the spinel $MnFe_2O_4$. Peaks at (220), (311), (400), (511), (440) and (533) are typical diffraction peaks of $MnFe_2O_4$ phase. Debye-Scherrer's formula is used for the calculation of average crystallite size as given below:

$$D = \frac{0.9\,\lambda}{\beta \cos\theta} \tag{1}$$

The average crystallite size of $MnFe_2O_4$ and ZrO_2 phase is about 9 and 4 nm, respectively. The average crystallite size is calculated after subtraction of instrumental broadening and error bar estimate ± 0.5-1 nm for ZrO_2 phase and ± 1-3 nm for the $MnFe_2O_4$ phase. Figures 2 (b) shows the selected area electron diffraction (SAED) of ZrO_2 coated $MnFe_2O_4$ nanoparticles as analyzed by using software "PASAD" [22]. The presence of sharp diffraction rings signify the crystalline nature of the nanoparticles. The PASAD evaluation of the SAED signify the presence of two different

crystalline species such as $MnFe_2O_4$ (core of the nanoparticles) and ZrO_2 (coating material), which is in good agreement with the XRD findings. Figure 2 (c) and (d) represent the transmission electron microscopy (TEM) images of ZrO_2 coated $MnFe_2O_4$ nanoparticles at 50 and 20 nm scales, respectively. TEM images show that ZrO_2 coated $MnFe_2O_4$ nanoparticles are spherical in shape and less agglomerated. Arrow in Fig. 4 (d) indicates the presence of ZrO_2 coating material.

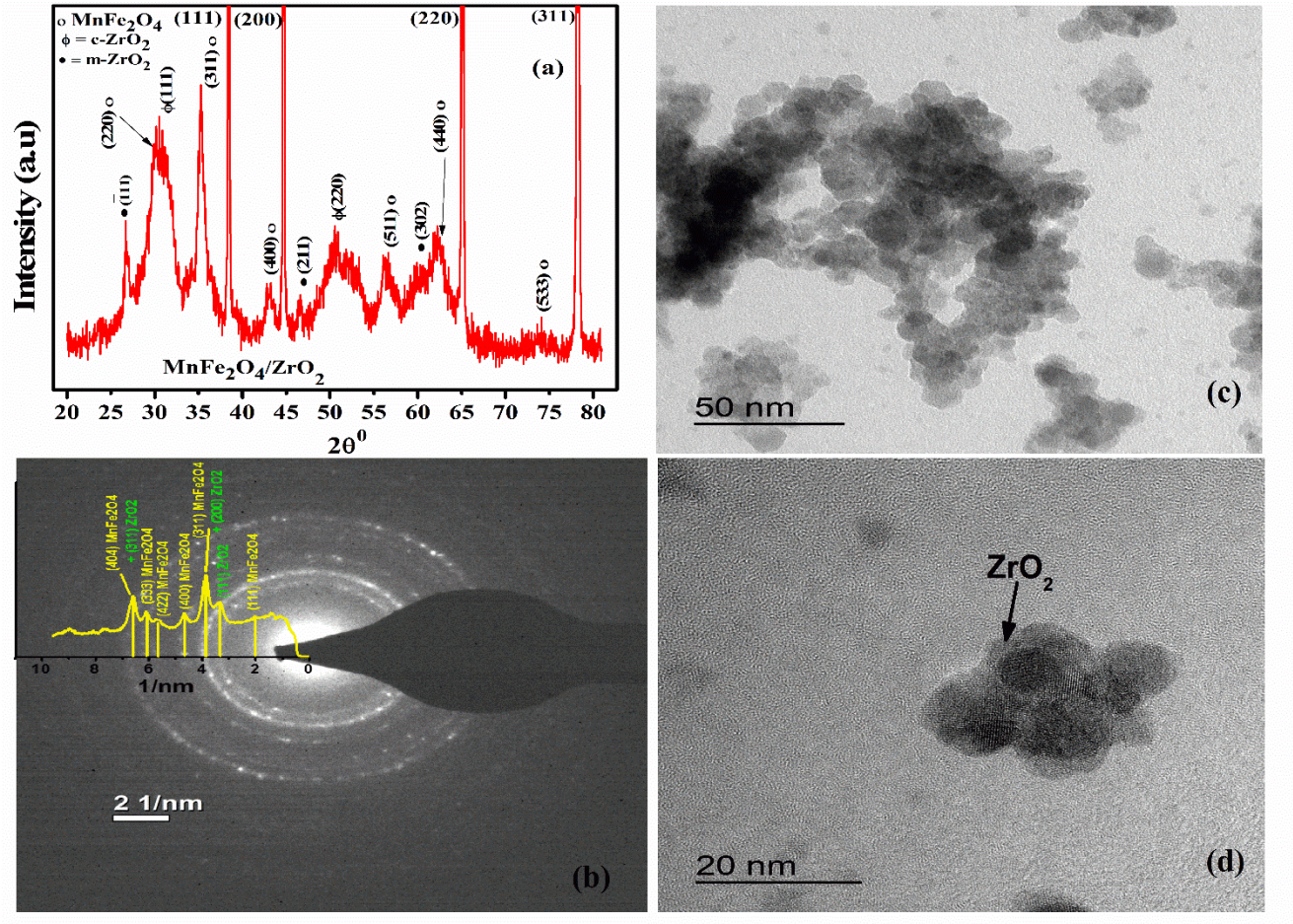

Fig. 2: (a) XRD scan of ZrO_2 coated $MnFe_2O_4$ nanoparticles, (b) selected area electron diffraction analyzed by software "PASAD", (c) TEM image at 50 nm scale and (d) TEM image of at 20 nm scale for ZrO_2 coated $MnFe_2O_4$ nanoparticles. Arrow in panel (d) indicates the presence of ZrO_2 coating.

Fig. 3 shows the experimental (blue circles) and simulated (red solid line) zero field cooled (ZFC)/field cooled (FC) magnetization curves of ZrO_2 coated $MnFe_2O_4$ nanoparticles in the temperature range 5–300 K under applied field of 100 Oe.

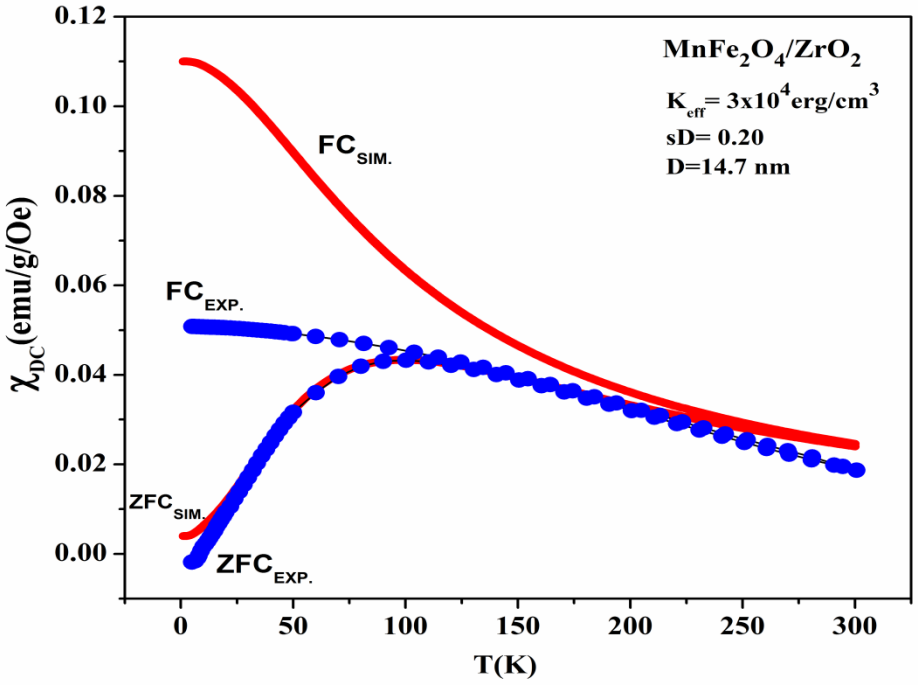

Fig. 3: Experimental (**blue circles)** and simulated (**red solid line**) ZFC/FC curves of ZrO_2 coated $MnFe_2O_4$ nanoparticles under applied field of 100 Oe.

ZFC curve shows a broad peak at 100 K which represents the average blocking temperature (T_B) of the nanoparticles. The experimental FC curve ($FC_{EXP.}$) becomes flat at low temperatures (below 100 K) as compared to simulated FC curve ($FC_{SIM.}$) which is due to the presence of interparticle interactions and/or surface spins disorder. Below T_B (ZFC), the nanoparticles spins are blocked along their random anisotropy axes and above T_B, the thermal energy is exceeded to anisotropy energy barrier and nanoparticles evolve in to the superparamagnetic state, which is also evident by the converging ZFC and FC curves above T_B [23]. For simulation (represented by red line in Fig. 3), we have adopted the Neel-Brown relaxation model by taking into account an uniaxial anisotropy [24,

25]. The log-normal distribution function of particle volumes was used for corresponding to their respective blocking temperatures T_B is given as,

$$(T_B)dT_B = \frac{1}{\sqrt{2\pi\sigma_{T_B}^2}}\frac{1}{T_B}exp\left(-\frac{\ln^2\frac{T_B}{<T_B>}}{2\sigma_{T_B}^2}\right)dT_B \quad (2)$$

The relationship between average blocking temperature $<T_B>$ and average particle volume <V> is given as:- $<V> = \frac{\pi < d >^3}{6}$ and $< T_B > = \frac{k_{eff}}{k_B \ln(\frac{\tau_m}{\tau_0})} < V >$. Where d is the diameter of the nanoparticle and σ_{TB} is the standard deviation in the blocking temperature. The ZFC/FC susceptibility by a SQUID magnetometer rely on the characteristic measurement time τ_m= 100 s as compared to the atomic spin precession time $\tau_0=10^{-10}$ s. For ZFC curve, which only represents the behavior of non-interacting, ZFC susceptibility is given by [26],

$$\chi_{ZFC}(T) = \frac{{M_S}^2}{3K_{eff}}[\ln\left(\frac{\tau_m}{\tau_0}\right)\int_0^T\frac{T_B}{T}f(T_B)dT_B + \int_T^\infty f(T_B)dT_B] \quad (3)$$

For a temperature "T", the 1st and the 2nd terms in the Eq. 3 are for the un-blocked superparamagnetic (T_B <T) and blocked nanoparticles (T_B >T), respectively. By using the assumptions of the same model, the FC susceptibility can be written as [26],

$$\chi_{FC}(T) = \frac{{M_S}^2}{3K_{eff}}\ln\left(\frac{\tau_m}{\tau_0}\right)[\frac{1}{T}\int_0^T T_B f(T_B)dT_B + \int_T^\infty f(T_B)dT_B] \quad (4)$$

The best fit gives the value of effective anisotropy energy-density K_{eff} = 3x10^{04} erg/cm^3 which is very close to the bulk value (K_{bulk} = 2.5x10^{04} erg/cm^3) and it shows weak contribution of surface anisotropy [27, 28]. Approximately same size polyvinylpyrrolidone coated $MnFe_2O_4$ nanoparticles showed K_{eff} = 1.42x10^{06} erg/cm^3 which is significantly higher than bulk value which is due to strong

magnetic coupling between ordered core and disordered surface spins [29]. Aslibeiki *et al.*[30] reported higher K_{eff} value for triethylene coated $MnFe_2O_4$ and attributed it to size and surface effects. All these reported results proved that other non-magnetic coating enhanced the surface anisotropy of $MnFe_2O_4$ nanoparticles and did not overcome the interaction between nanoparticles. However in our case, ZrO_2 coated $MnFe_2O_4$ nanoparticles showed K_{eff} nearly equal to that of bulk value of $MnFe_2O_4$ by reducing the interactions among the nanoparticles. The $FC_{EXP.}$ and $FC_{SIM.}$ curves a show difference which arises because our model covers only non-interacting particles. The $FC_{EXP.}$ curve tends to saturate below T_B which is typical for interacting particles and hint for the presence of super spin-glass state.

Fig. 4 (a), (b) and (c) shows the M-H loop at 5 K, T-dependent saturation magnetization (M_S) with the "Bloch's law" fit (red dashed line) and T-dependent coercivity (H_C) of ZrO_2 coated $MnFe_2O_4$ nanoparticles, respectively.

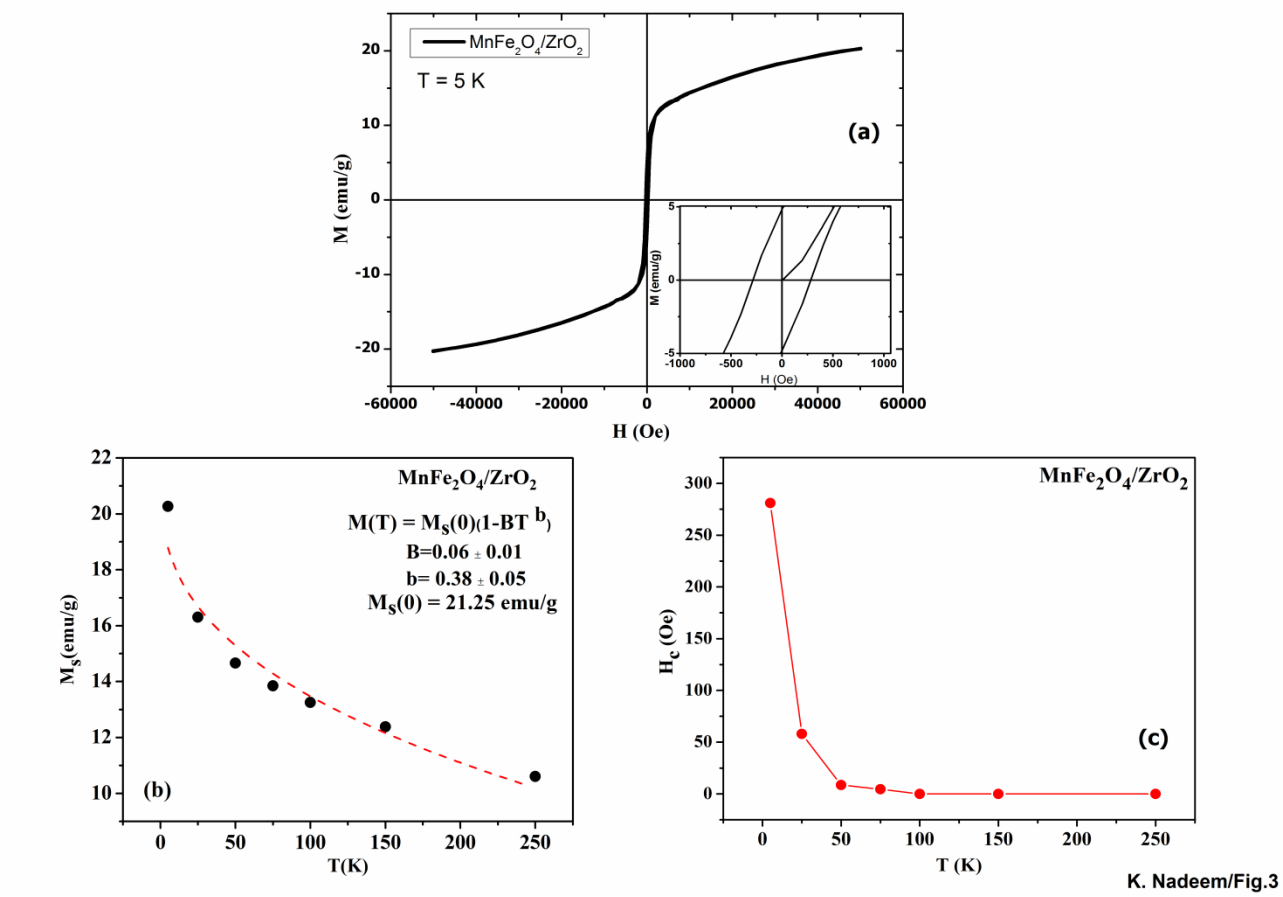

Fig. 4: (a) M-H loop at 5 K with inset which shows the expanded view of coercivity region, (b) T-dependent saturation magnetization of ZrO_2 coated $MnFe_2O_4$ nanoparticles fitted with Bloch's law (red dashed line) and (c) T-dependent coercivity of ZrO_2 coated $MnFe_2O_4$ nanoparticles.

It is evident that the M-H loop at 5 K is not saturated even at high field of ± 5T. The non-saturation of magnetization in small ferrite nanoparticles is due to uncompensated disordered surface spins which require rather high field to saturate as compared to aligned core spins. It has been reported that $MnFe_2O_4$ nanoparticles showed superparamagnetic behavior at 50 nm [31]. Above 100 K, coercivity gets vanish ($H_C \rightarrow 0$ Oe) which indicates the presence of superparamagnetic state and it is in accordance with the average blocking temperature T_B = 100 Oe as obtained from the ZFC/FC. The maximum value of M_S was found at 5 K [M_S (5 K) = 20.29 emu/g] which is well below the bulk value [M_S = 80 emu/g]. The reduction of M_S value in ferrite nanoparticles is well understood and is

attributed to disordered surface spins. The M_S value decreases with increasing temperature which is due to a more randomly oriented spin structure at high temperatures [32-34].

The M_S value exhibits a monotonous increase toward T→ 0 K and excitation of spin waves is responsible for this behavior. Bloch's law as given in Eq. 5 usually explains the temperature dependent saturation magnetization (Ms) of bulk ferromagnetic material,

$$M_S(T) = M_S(0)(1 - BT^b) \quad (5)$$

Where M_S (0) is the extrapolated M_S value at 0 K, B is the Bloch's constant and b is Bloch's exponent (for bulk material b = 1.5). Usually nanoparticles show deviation from Bloch's law at low temperatures due to presence of interparticle interactions, finite size effects and disordered surface spins [35, 36]. Fig. 4 (b) shows the Bloch's law fit for M_S vs. T data by using Eq. 5. The best fit shows divergence at low temperatures due to the sharp increase of M_S at 5 K. Usually M_S shows saturation or even decreasing behavior at low temperatures for ferrite nanoparticles having intense surface spins disorder [37, 38]. In our case, M_S increases monotonically with lowering temperature which is caused by reduced surface spins disorder due to ZrO_2 coating. The fitted parameters for the Bloch's law are B = 0.06 K^{-b} and b = 0.38 respectively. The increased value of B is due to decrease in e□ective exchange coupling (J) in these nanoparticles and smaller value of b is due to finite size effects.

In Fig. 4 (c), it is revealed that H_C exhibits a sharp increase below 25 K which is due to surface spin freezing which gives contribution of additional surface anisotropy at low temperatures. Dipolar-interactions between particles, size distributions and structural inhomogeneity can also affect the H_C of ferrite nanoparticles. We have tried to fit our experimental data with Kneller's law but the fitting failed due to sharp increase of H_C at low temperatures. The same results were reported by Shendurk

et al. [39] during the study of H_C of γ-Fe_2O_3 nanoparticles fitted with Kneller's law. They reported that temperature dependency of anisotropy and surface effects are responsible for such behavior.

We have also measured the ac susceptibility to understand the ac dynamics of the $MnFe_2O_4$ nanoparticles. Coating can influence the frequency dependent ac susceptibility and also effect the blocking temperature of nanoparticles. Generally, the relaxation time of blocked nanoparticles is mainly determined by the energy barrier ($E_a = K_{eff}V$) and the magnetic state of nano-magnets could be interrogated by the frequency sweep ($\omega = 1/t_m$) of ac susceptibility measurements. Fig. 5 (a, b) shows the in-phase (χ') and out-of-phase part (χ'') of ac susceptibility from 5 to 300 K under an ac applied field of 5 Oe at frequencies (f) = 1, 10, 100 and 1000 Hz.

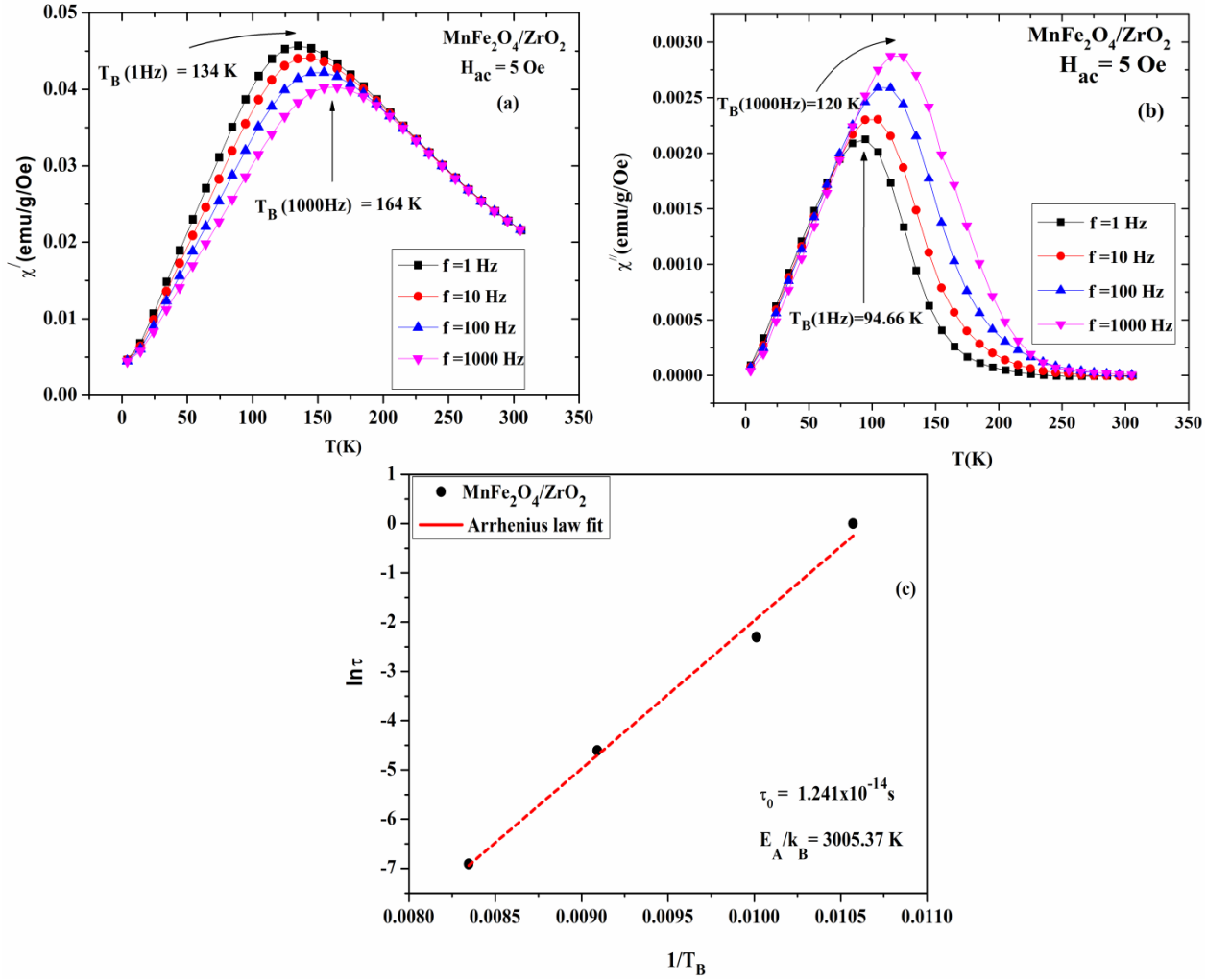

Fig. 5: (a) In-phase, (b) out-of-phase part of ac susceptibility at various excitation frequencies and (c) Arrhenius law fit for ZrO_2 coated $MnFe_2O_4$ nanoparticles.

The T_B peak increases with increasing frequency due to the change of probing time ($t_m = 1/\omega$) with applied frequency. For χ', the T_B shifts from 134 to 165 K as the frequency is increased from 1 Hz to 1000 Hz. The T_B value in ZFC/FC scan (Fig. 3) was about 100 K, lower than the T_B found in ac susceptibility, which is due to the T_B-shift by the applied DC-field H_{dc} = 100 Oe in ZFC/FC measurement, which is missing in ac susceptibility measurement. The maximum of χ'' reflects the energy dissipation in the system. This χ'' peak lies near the turning point of in-phase part of ac susceptibility (according to Hilbert transform), is therefore always left from the maximum peak of χ' for log-norm distributed volumes, therefore the evaluation of out-of-phase part reflects much better the relaxation time τ for fitting the various relaxation models. For complete description of dynamics of our nanoparticles, we have tried to fit the f-dependent shift of the T_B-peak in the χ'' by using Arrhenius law which is used for thermal excitation of single-barrier blocked non-interacting particles and can be written as

$$\tau_m = \tau_0 \exp\left(\frac{E_a}{k_B T_B}\right) \quad (6)$$

Where "E_a", "k_B", "T_B" and "τ_o" represent the activation energy, Boltzmann constant, blocking temperature deduced from ac susceptibility and the atomic spin-flip time of nanoparticles, respectively [40]. The values of parameters as deduced from such a fit are $\tau_o = 1.24 \times 10^{-14}$ s and E_A/k_B= 3005 K. It shows that our nanoparticles do not exactly follow Arrhenius law but the slightly lower value of τ_o showed the existence of weak interparticle interactions in our nanoparticles [41, 42]. In the literature, the frequency dependent ac susceptibility study of bare and tri-ethylene glycol coated $MnFe_2O_4$ nanoparticles showed super spin-glass state due to strong interactions among the nanoparticles [43-46]. However, our ac susceptibility data proved that ZrO_2 coating has reduced the

surface disorder and interactions between $MnFe_2O_4$ nanoparticles and prevents them to create a spin-glass behaviour.

Superparamagnetism and spin-glass behaviour can be distinguishable by analysing ZFC and FC relaxation curves. Superparamagnetic system shows slow spin relaxation in only FC, while spin-glass system exhibits slow relaxation in both ZFC and FC protocols. Therefore, we have done only ZFC relaxation curve which is specific for a spin-glass system. However, in addition to spin-glass systems, some other disordered systems can also show slow spin relaxation in FC protocol that can be analysed by shape parameter found in different relaxation laws. For different disordered systems, the shape parameter (β) lies between 0 and 1. The β value for spin-glass system lies in the range of 0.2 to 0.6 [47]. Wang *et al.* [48] reported the value of shape parameter (β = 0.52) during the study of spin glass state in La-Fe-Mn-Si alloy which lie at below freezing temperature. Therefore, spin glass state depends on the value of shape parameter β. To investigate the possibility of spin-glass state in our nanoparticles, we have measured only magnetic relaxation below T_B after ZFC protocol, which is typical for disorder or spin-glass system. Fig. 6 shows the magnetic relaxation curve of ZrO_2 coated $MnFe_2O_4$ after zero-field-cooling at T = 5 K and subsequent switch-on of a magnetic field of 100 Oe. It reveals slow spin "creeping" which is probably due to surface disorder and magnetic frustration. Commonly two models are used to fit the magnetic relaxation data namely logarithmic relaxation decay and stretched exponential decay model [49]. We have used stretched exponential law to fit the relaxation curve given as:

$$M = M_2 - (M_2 - M_1)\exp\left[-(t/\tau)^{\beta}\right] \quad (7)$$

Where, M_2 and M_1 are the final and initial magnetization values of the relaxation data, τ is used for the mean relaxation time and β represents the shape parameter.

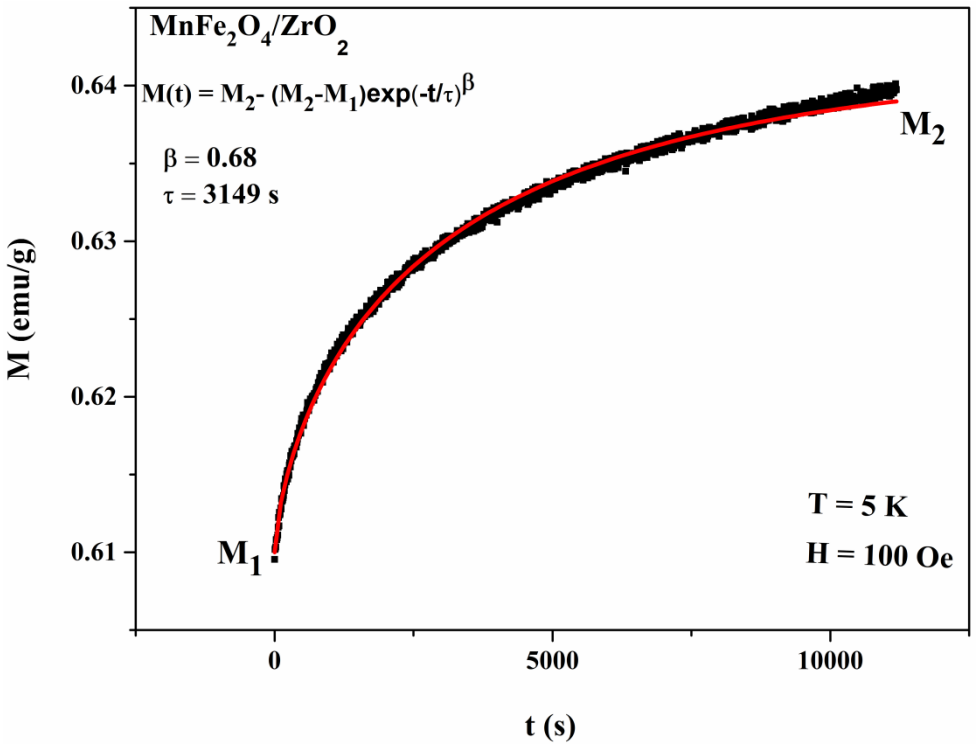

Fig. 6: Magnetic relaxation curve of ZrO_2 coated $MnFe_2O_4$ after zero-field-cooling at T = 5 K, a subsequent switch-on of a magnetic field of 100 Oe.

The best fit of Eq. 8 reveals parameters τ = 3149 s and β = 0.7. The fitted shape parameter value (β = 0.7) lies outside the spin-glass regime (0.2 – 0.6). The higher value of β shows that our system does not fall in spin-glass state but the presence of slow relaxation in ZFC protocol cannot exclude the existence of disorder in our system. However, this disorder is not significant to produce a spin-glass state, which is consistent with effective anisotropy constant close to the bulk value, sharp increase of M_S at low temperatures and spin-flip time in Arrhenius law fit. Therefore, our nanoparticles exhibit weak interparticle interactions and weak surface disorder which are not sufficient to produce spin-glass state (surface or super spin-glass state). The reduction in interparticle

interactions and weak surface effects are probably caused by ZrO_2 coating in these fine $MnFe_2O_4$ nanoparticles.

Conclusions

$MnFe_2O_4$ nanoparticles coated by ZrO_2 were successfully synthesized by using microwave plasma synthesis method. XRD analysis confirmed the crystalline $MnFe_2O_4$ and ZrO_2 phases which are further signified by selected area electron diffraction evaluation. Flattening of $FC_{EXP.}$ curve showed an existence of weak interparticle interactions. The simulated $K_{eff} = 3x10^{04}$ erg/cm^3 value is slightly higher than the bulk value which ensures the weak surface anisotropy in these nanoparticles. Saturation magnetization showed an increased value at low temperature due to the reduced surface spins disorder caused by ZrO_2 coating. Arrhenius law fit provided the value of spin flip time (τ_o =1.24 x 10^{-14} s) close to atomic spin-flip time and is attributed to weak interparticle interactions. The value of shape parameter in ZFC relaxation curve revealed the existence of disorder but no spin-glass state. In conclusion, ZrO_2 coated fine $MnFe_2O_4$ nanoparticles exhibit reduced interparticle interactions and surface effects which were not sufficient to produce spin-glass behaviour and all this is attributed to non-magnetic ZrO_2 coating.

Acknowledgement

K. Nadeem acknowledges International Islamic University for providing research funds under project no. IIUI/ORIC/RP/HRSC/2016-518.

List of Figures:

References

[1] Q.-m. Wei, J.-b. Li, Y.-j. Chen, Y.-s. Han, X-ray study of cation distribution in $NiMn_{1-x}Fe_{2-x}O_4$ ferrites, Mater. Charact., 47 (2001) 247-252.

[2] J. A. Taylor, S. T. Reczek, A. Rosen, Soft ferrite processing, Am. Ceram. Soc. Bull., 74 (1995) 91-94.

[3] M. Rozman, M. Drofenik, Sintering of nanosized MnZn ferrite powders, J. Am. Ceram. Soc., 81 (1998) 1757-1764.

[4] S. Chen, S. Chang, I. Lin, The influence of grain boundary internal stress on permeability: temperature curve for Mn–Zn ferrites, J. Magn. Magn. Mater., 209 (2000) 193-196.

[5] R. Kadam, A. Biradar, M. Mane, S. E. Shirsath, Sol-gel auto-combustion synthesis of $Li_{3x}MnFe_{2-x}O_4$ and their characterizations, J. Appl. Phys., 112 (2012) 043902.

[6] S. E. Shirsath, B. Toksha, R. Kadam, S. Patange, D. Mane, G. S. Jangam, A. Ghasemi, Doping effect of Mn^{2+} on the magnetic behavior in Ni–Zn ferrite nanoparticles prepared by sol–gel auto-combustion, J. Phys. Chem., 71 (2010) 1669-1675.

[7] R. Topkaya, Ö. Akman, S. Kazan, B. Aktaş, Z. Durmus, A. Baykal, Surface spin disorder and spin-glass-like behaviour in manganese-substituted cobalt ferrite nanoparticles, J. Nanopart. Res., 14 (2012) 1156.

[8] M. G. Naseri, E. B. Saion, H. A. Ahangar, M. Hashim, A. H. Shaari, Synthesis and characterization of manganese ferrite nanoparticles by thermal treatment method, J. Magn. Magn. Mater., 323 (2011) 1745-1749.

[9] W. Nunes, A. Gomes, R. Rapp, M. Novak, Specific heat and magnetization studies of spin-glass like transition in nanogranular $Cu_{90}Co_{10}$ ribbon, J. Magn. Magn. Mater., 370 (2014) 116-121.

[10] J. Dormann, R. Cherkaoui, L. Spinu, M. Nogues, F. Lucari, F. D'Orazio, D. Fiorani, A. Garcia, E. Tronc, J. Jolivet, From pure superparamagnetic regime to glass collective state of magnetic moments in γ-Fe_2O_3 nanoparticle assemblies, J. Magn. Magn. Mater., 187 (1998) L139-L144.

[11] R. H. Kodama, A. E. Berkowitz, Atomic-scale magnetic modeling of oxide nanoparticles, Phys. Rev. B, 59 (1999) 6321.

[12] L. N. Lartigue, P. Hugounenq, D. Alloyeau, S. P. Clarke, M. Lévy, J.-C. Bacri, R. Bazzi, D. F. Brougham, C. Wilhelm, F. Gazeau, Cooperative organization in iron oxide multi-core nanoparticles potentiates their efficiency as heating mediators and MRI contrast agents, ACS Nano, 6 (2012) 10935-10949.

[13] R.-R. Gao, Y. Zhang, W. Yu, R. Xiong, J. Shi, Superparamagnetism and spin-glass like state for the $MnFe_2O_4$ nano-particles synthesized by the thermal decomposition method, J. Magn. Magn. Mater., 324 (2012) 2534-2538.

[14] S. Ghosh, P. C. Patel, P. Srivastava, Hysteresis in magnetoresistance and formation of spin glass like structure in PVA capped Fe_3O_4, J. Mater. Sci.- Mater. Electron., 28 (2017) 15284-15292.

[15] B. Aslibeiki, P. Kameli, M. Ehsani, H. Salamati, G. Muscas, E. Agostinelli, V. Foglietti, S. Casciardi, D. Peddis, Solvothermal synthesis of $MnFe_2O_4$ nanoparticles: the role of polymer coating on morphology and magnetic properties, J. Magn. Magn. Mater., 399 (2016) 236-244.

[16] A. ur Rashid, A. Humayun, S. Manzoor, $MgFe_2O_4/ZrO_2$ composite nanoparticles for hyperthermia applications, J. Magn. Magn. Mater., 428 (2017) 333-339.

[17] G. S. Chaubey, J.-K. Kim, Structure and Magnetic Characterization of Core-Shell Fe@ZrO_2 Nanoparticles Synthesized by Sol-Gel Process, Bull. Korean Chem. Soc., 28 (2007) 2279-2282.

[18] S. Larumbe, J. Pérez-Landazábal, J. Pastor, C. Gomez-Polo, Sol-gel $NiFe_2O_4$ nanoparticles: Effect of the silica coating, J. Appl. Phys., 111 (2012) 103911.

[19] X. H. Xu, X.-L. Li, H.-S. Wu, Effect of ZrO_2 layer thickness on microstructure and magnetic properties of $FePt/ZrO_2$ multilayers, Mater. Sci. Eng., B, 121 (2005) 183-186.

[20] D. Vollath, D. V. Szabó, The Microwave plasma process–a versatile process to synthesise nanoparticulate materials, J. Nanopart. Res., 8 (2006) 417-428.

[21] D. V. Szabó, S. Schlabach, Microwave plasma synthesis of materials—From physics and chemistry to nanoparticles: A materials scientist's viewpoint, Inorganics, 2 (2014) 468-507.

[22] C. Gammer, C. Mangler, C. Rentenberger and H.P. Karnthaler: Quantitative local profile analysis of nanomaterials by electron diffraction. Scripta Materialia 63 (2010) 312-315.

[23] Y. Köseoğlu, F. Alan, M. Tan, R. Yilgin, M. Öztürk, Low temperature hydrothermal synthesis and characterization of Mn doped cobalt ferrite nanoparticles, Ceram. Int., 38 (2012) 3625-3634.

[24] L. Néel, Théorie du traînage magnétique de diffusion, J. phys. radium, 13 (1952) 249-264.

[25] W. Brown, I. Krivorotov, N. Emley, A. Garcia, J. Sankey, S. Kiselev, D. Ralph, R. Buhrman, Z. Li, S. Zhang, Temperature dependence of spin-transfer-induced switching of nanomagnets, J. Phys. Rev., 130 (1963) 1677-1686.

[26] J. Denardin, A. Brandl, M. Knobel, P. Panissod, A. Pakhomov, H. Liu, X. Zhang, Thermoremanence and zero-field-cooled/field-cooled magnetization study of $Co_x(SiO_2)_{1-x}$ granular fil, Phys. Rev. B, 65 (2002) 064422.

[27] P.T. Phong, P. Nam, D. Tung, I.-J. Lee, N. Phuc, Studies of the magnetic properties and specific absorption of $Mn_{0.3}Zn_{0.7}Fe_2O_4$ nanoparticles, J. Electron. Mater., 44 (2015) 287.

[28] S. Yoon, K. M. Krishnan, Temperature dependence of magnetic anisotropy constant in manganese ferrite nanoparticles at low temperature, J. Appl. Phys., 109 (2011) 07B534.

[29] R. Topkaya, U. Kurtan, A. Baykal, M. S. Toprak, Polyvinylpyrrolidone (PVP)/$MnFe_2O_4$ nanocomposite: Sol–Gel autocombustion synthesis and its magnetic characterization, Ceram. Int., 39 (2013) 5651-5658.

[30] B. Aslibeiki, P. Kameli, H. Salamati, The effect of dipole-dipole interactions on coercivity, anisotropy constant, and blocking temperature of $MnFe_2O_4$ nanoparticles, J. Appl. Phys., 119 (2016) 063901.

[31] T. Sato, T. Iijima, M. Seki, N. Inagaki, Magnetic properties of ultrafine ferrite particles, J. Magn. Magn. Mater., 65 (1987) 252-256.

[32] J. D. Starr, Janus-type ceramic nanomaterials: Anisotropic building blocks for the formation of new composites, in, University of Florida, 2014.

[33] B. Figgis, M. Hitchman, Ligand Field Theory and its Application", Wiley-VCH, New York, Singapore, Toronto, (2000).

[34] P. V. Hendriksen, S. Linderoth, P.-A. Lindgård, Finite-size modifications of the magnetic properties of clusters, Phys. Rev. B, 48 (1993) 7259.

[35] S. Linderoth, L. Balcells, A. Labarta, J. Tejada, P. Hendriksen, S. Sethi, Magnetization and Mössbauer studies of ultrafine Fe-C particles, J. Magn. Magn. Mater., 124 (1993) 269-276.

[36] F. Zeb, K. Nadeem, S. K. A. Shah, M. Kamran, I. H. Gul, L. Ali, Surface spins disorder in uncoated and SiO_2 coated maghemite nanoparticles, J. Magn. Magn. Mater., 429 (2017) 270-275.

[37] Y. Bai, J. Zhou, Z. Gui, Z. Yue, L. Li, Complex Y-type hexagonal ferrites: an ideal material for high-frequency chip magnetic components, J. Magn. Magn. Mater., 264 (2003) 44-49.

[38] M. George, A. M. John, S. S. Nair, P. Joy, M. Anantharaman, Finite size effects on the structural and magnetic properties of sol–gel synthesized $NiFe_2O_4$ powders, J. Magn. Magn. Mater., 302 (2006) 190-195.

[39] T. Shendruk, R. Desautels, B. Southern, J. Van Lierop, The effect of surface spin disorder on the magnetism of γ-Fe_2O_3 nanoparticle dispersions, Nanotechnology, 18 (2007) 455704.

[40] J. Dormann, D. Fiorani, E. Tronc, Advances in chemical physics, Vol. XCVII, Eds. I. Prigogine y Stuart A. Rice, John Wiley and Sons, 283 (1997).

[41] S. H. Masunaga, R. d. F. Jardim, P. F. P. Fichtner, J. Rivas, Role of dipolar interactions in a system of Ni nanoparticles studied by magnetic susceptibility measurements, Phys. Rev. B, 80 (2009) 184428.

[42] C. Cannas, G. Concas, D. Gatteschi, A. Falqui, A. Musinu, G. Piccaluga, C. Sangregorio, G. Spano, Superparamagnetic behaviour of γ-Fe_2O_3 nanoparticles dispersed in a silica matrix, Phys. Chem. Chem. Phys., 3 (2001) 832-838.

[43] B. Aslibeiki, P. Kameli, H. Salamati, M. Eshraghi, T. Tahmasebi, Superspin glass state in $MnFe_2O_4$ nanoparticles, J. Magn. Magn. Mater., 322 (2010) 2929-2934.

[44] M. Suzuki, S. I. Fullem, I. S. Suzuki, L. Wang, C.-J. Zhong, Observation of superspin-glass behavior in Fe_3O_4 nanoparticles, Phys. Rev. B, 79 (2009) 024418.

[45] J. Alonso, M. Fdez-Gubieda, J. Barandiarán, A. Svalov, L. F. Barquín, D. A. Venero, I. Orue, Crossover from superspin glass to superferromagnet in Fe_xAg_{100-x} nanostructured thin films ($20 \leq x \leq 50$), Phys. Rev. B, 82 (2010) 054406.

[46] C. E. Botez, A. H. Adair, R. J. Tackett, Evidence of superspin-glass behavior in $Zn_{0.5}Ni_{0.5}Fe_2O_4$ nanoparticles, J. Phys.: Condens. Matter., 27 (2015) 076005.

[47] A. Bhattacharyya, S. Giri, S. Majumdar, Spin-glass-like state in GdCu: Role of phase separation and magnetic frustration, Phys. Rev. B, 83 (2011) 134427.

[48] F. Wang, J. Zhang, Y.-f. Chen, G.-j. Wang, J.-r. Sun, S.-y. Zhang, B.-g. Shen, Spin-glass behavior in La $(Fe_{1-x}Mn_x)_{11.4}Si_{1.6}$ compounds, Phys. Rev. B, 69 (2004) 094424.

[49] D. S. Fisher, D. A. Huse, Ordered phase of short-range Ising spin-glasses, Phys. Rev. Lett., 56 (1986) 1601.

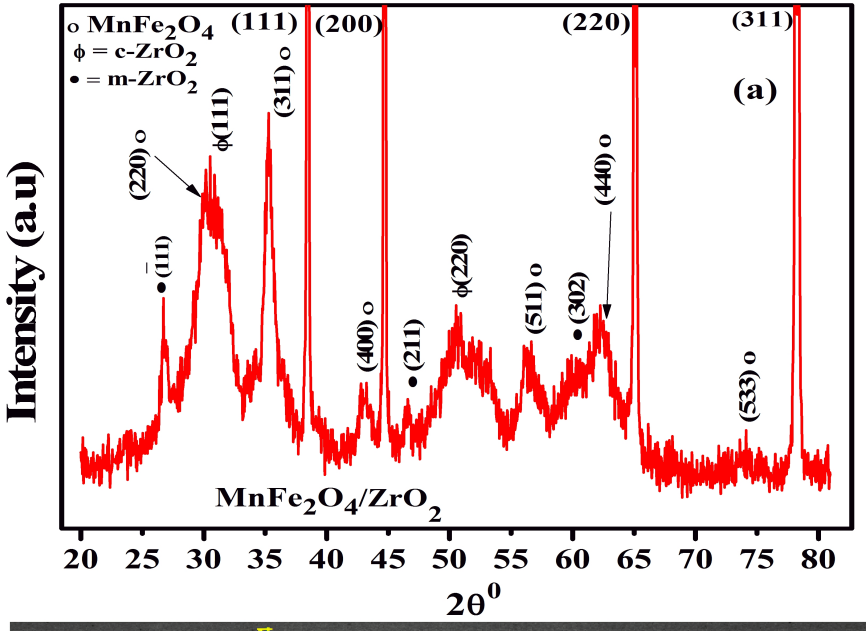
o MnFe2O4
ϕ = c-ZrO2
• = m-ZrO2
(111)
(200)
(220)
(311)
(a)
(220) o
• (111)
ϕ(111)
(311) o
(400) o
• (211)
ϕ(220)
(511) o
• (302)
(440) o
(533) o
MnFe2O4/ZrO2
Intensity (a.u)
20 25 30 35 40 45 50 55 60 65 70 75 80
2θ0

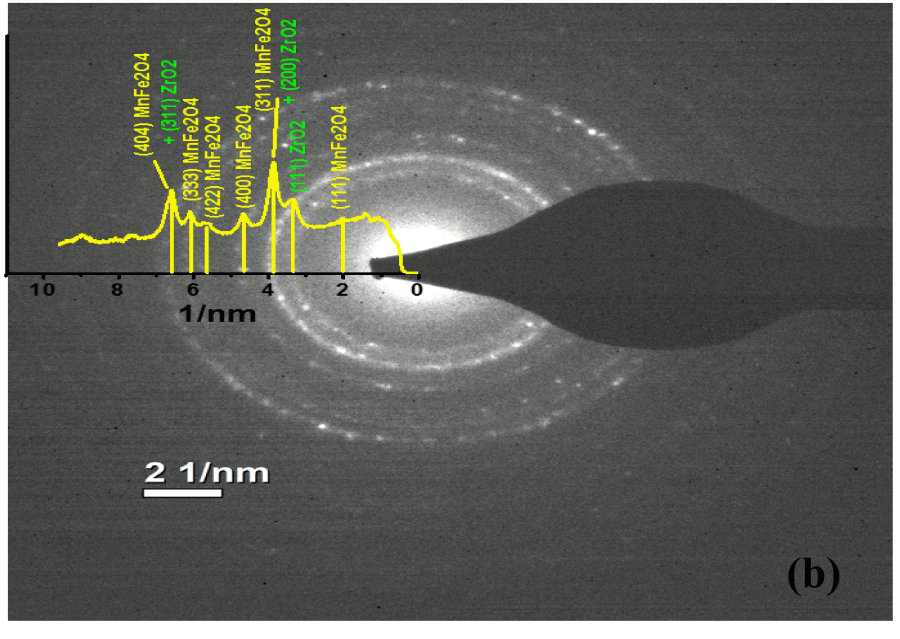
(404) MnFe2O4
+ (311) ZrO2
(333) MnFe2O4
(422) MnFe2O4
(400) MnFe2O4
(311) MnFe2O4
+ (200) ZrO2
(111) ZrO2
(111) MnFe2O4
10 8 6 4 2 0
1/nm
2 1/nm
(b)

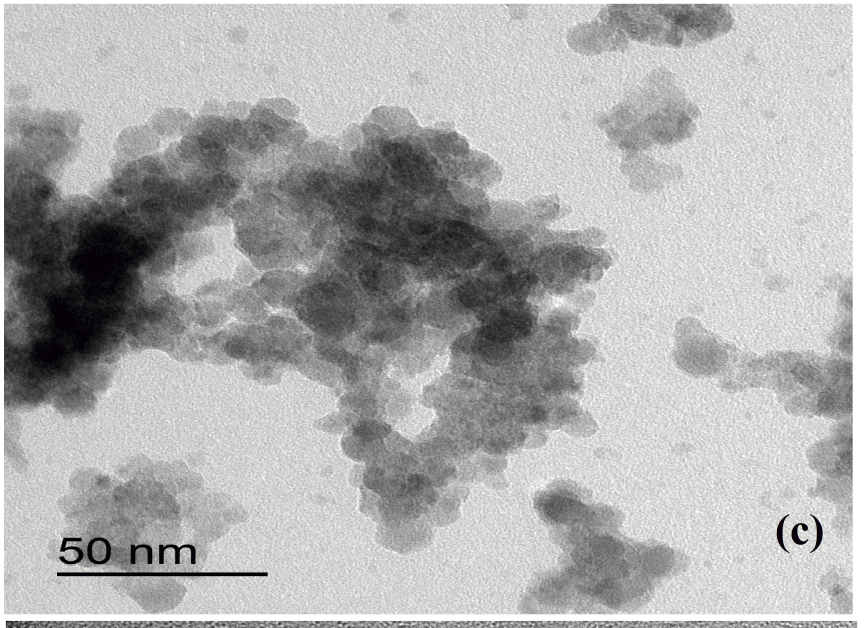
50 nm
(c)

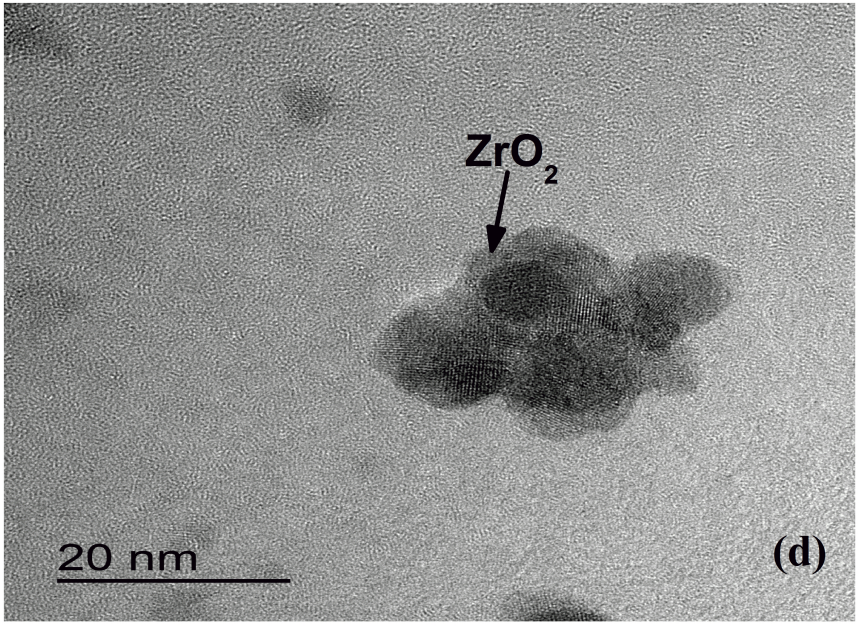
ZrO2
20 nm
(d)

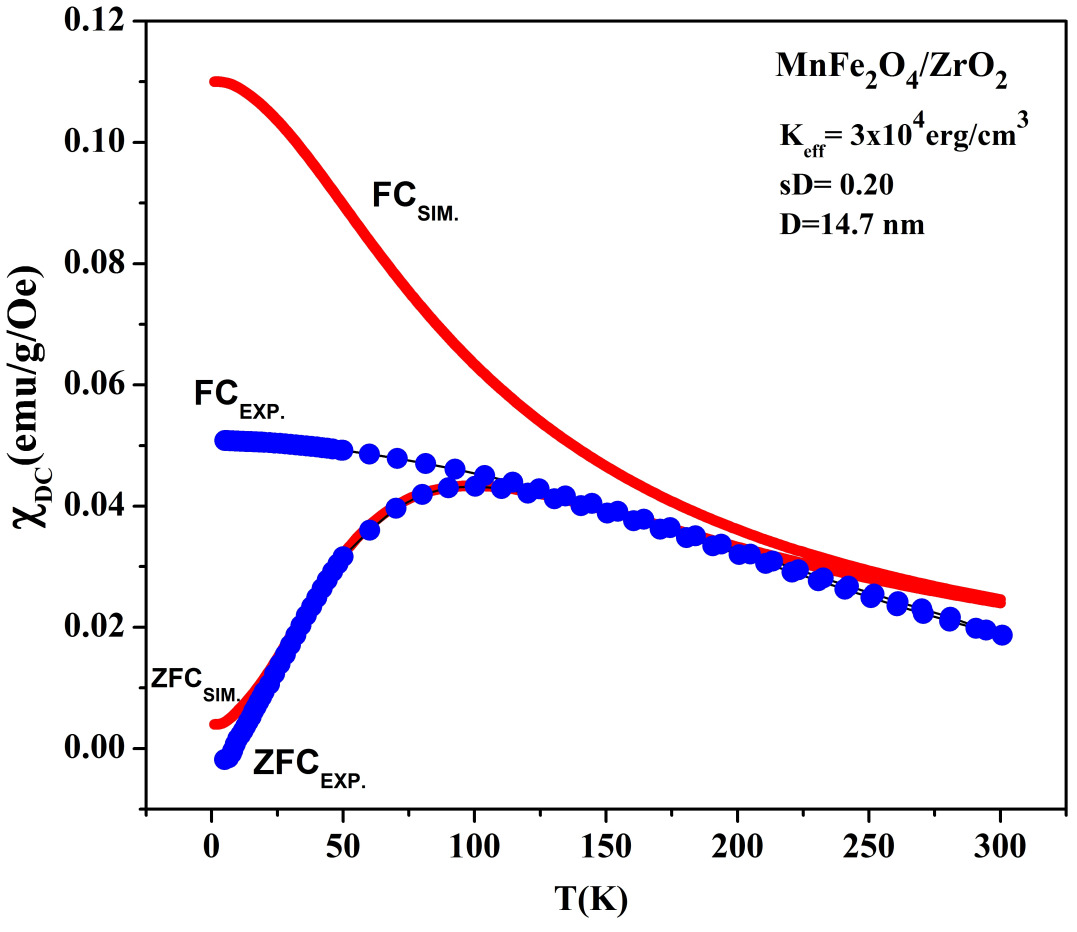

K.Nadeem/ Fig. 2

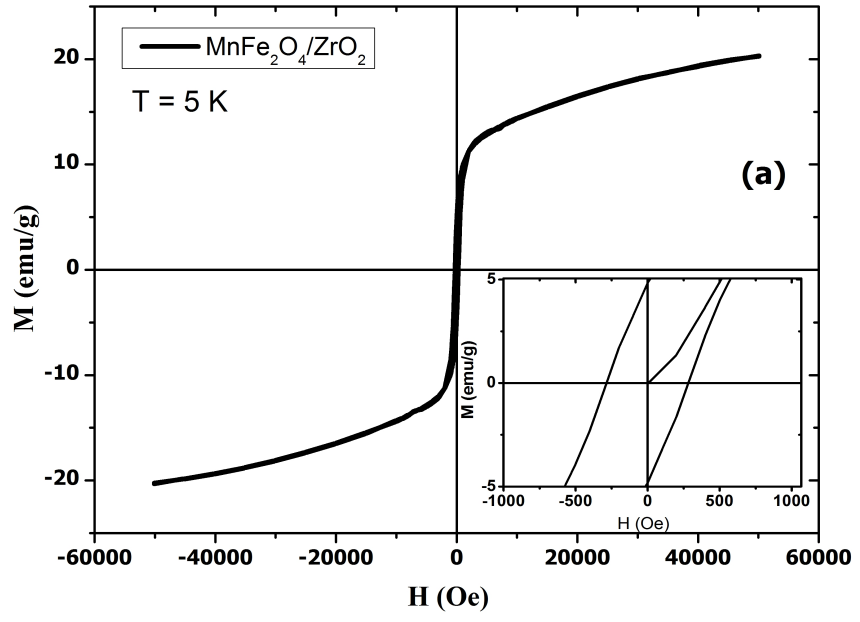

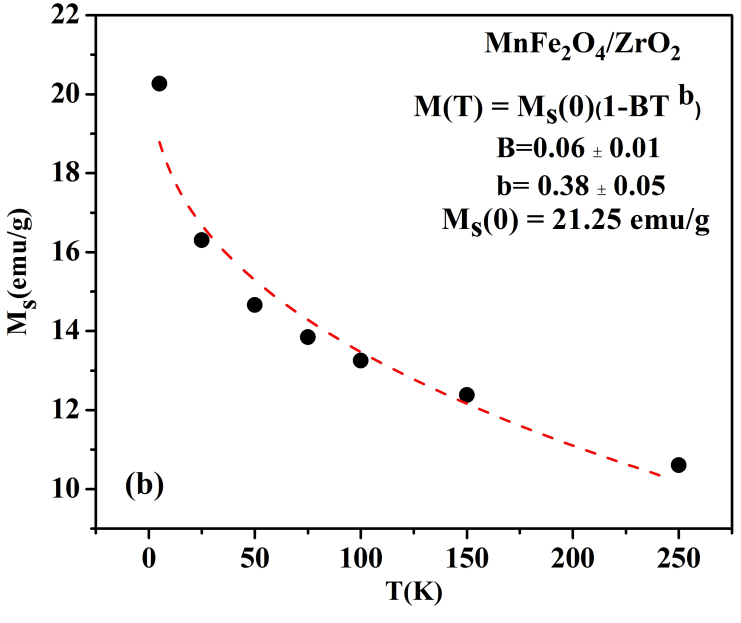

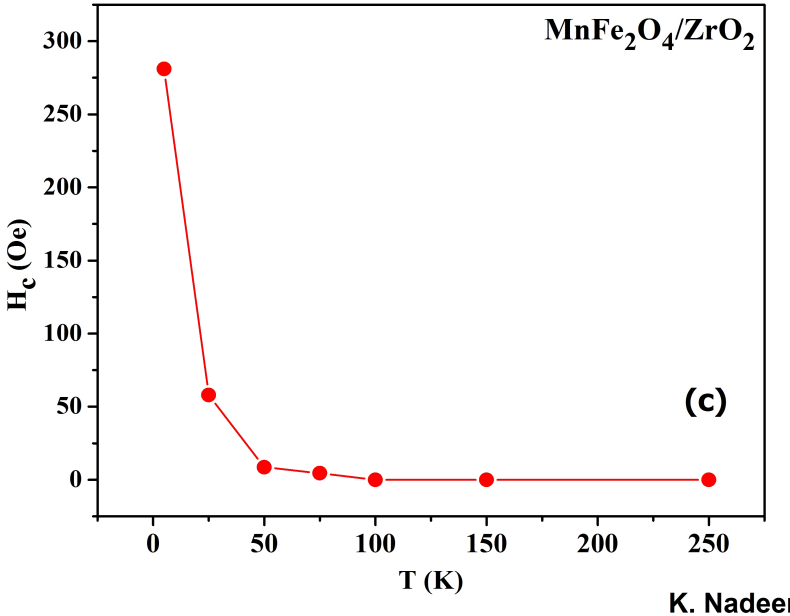

K. Nadeem/Fig.3

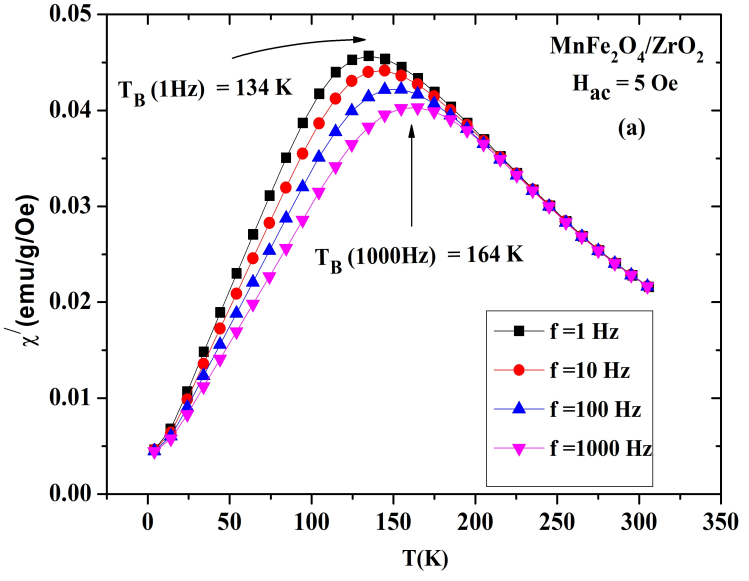

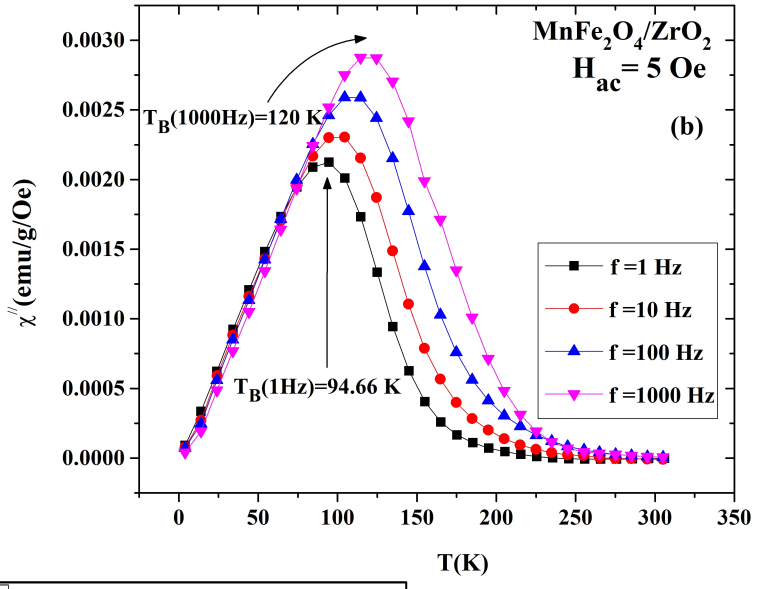

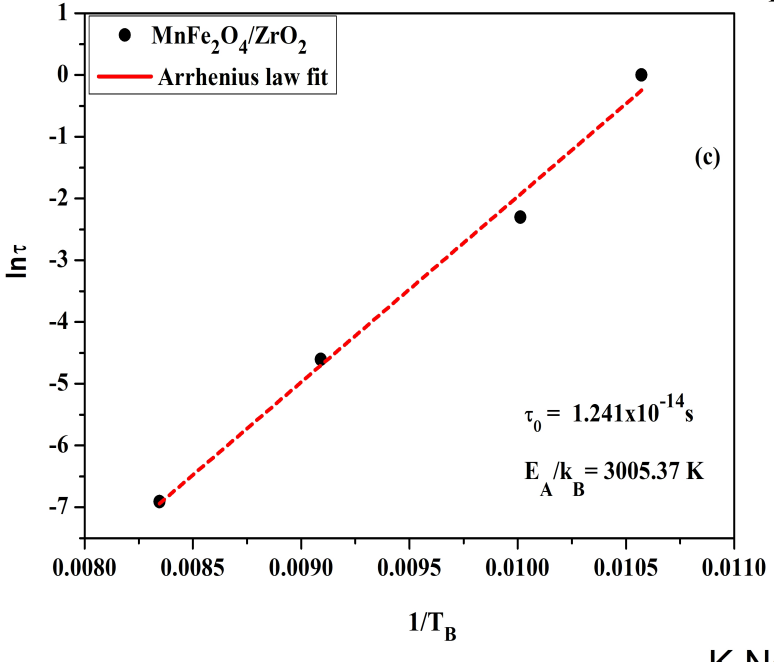

K.Nadeem/Fig. 4(a,b,c)

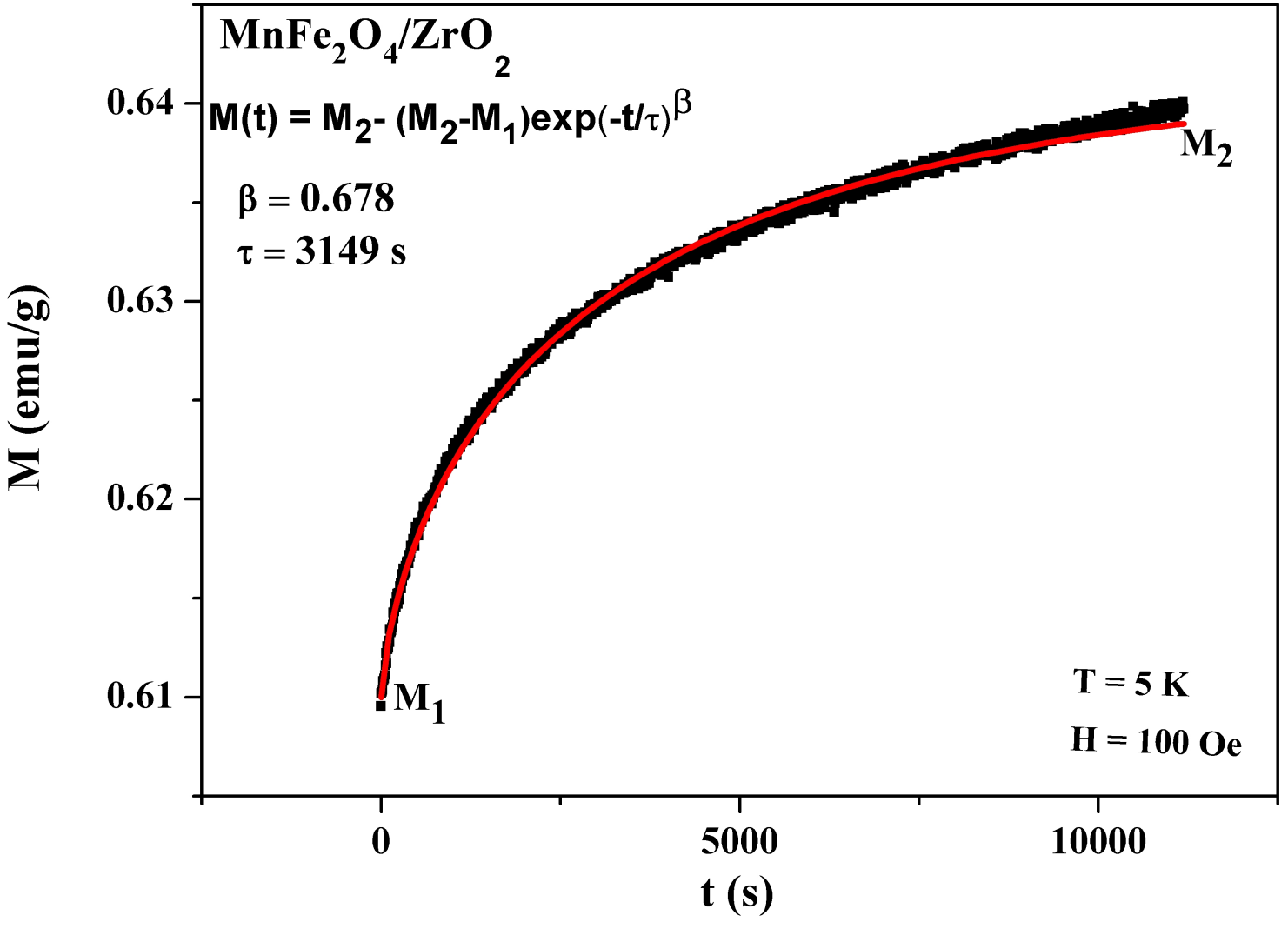
MnFe2O4/ZrO2
M(t) = M2- (M2-M1)exp(-t/τ)β
β = 0.678
τ = 3149 s
M2
M1
T = 5 K
H = 100 Oe
M (emu/g)
0.64
0.63
0.62
0.61
0
5000
10000
t (s)